Observations of thunderstorms on Jupiter: Storm activity in areas of cyclonic shear and near the centers of westward moving jets

Arthur E. Michalak*
Department of Physics and Program in Atmospheric & Oceanic Sciences
University of Colorado, Boulder, CO 80309

Sent 1 May 2004

Abstract

We present the frequency of occurrence, spatial distribution, and meteorology of jovian lightning storms retrieved from the Galileo Solid State Imager (SSI) in October and November of 1997. Storm occurrence in areas of cyclonic shear and near the centers of westward moving jets is discussed. An outline of relevant data of physical importance concerning Jupiter's storm activity is presented, with particular emphasis placed on the most appropriate observations made and the meteorology inferred from the probes findings.

1 Introduction

The study of lightning on Jupiter is interesting for several reasons. Firstly lightning on Jupiter indicates the presence of moist convection, an important element in atmospheric dynamics and energy transfer (Salby 1996). Secondly, lightning on Jupiter likely requires water in amounts that locally approach or exceed the solar value (Yair *et al.* 1995, Gibbard *et al.* 1996). Thirdly, lightning may contribute a significant role in the production of important trace species such as C_2H_2, HCN, and CO (Bar-Nun and Podolak 1985). Fourthly, cloud electrification is of interest for its own sake, and is not well understood (Golde 1977, Uman 1987). Lastly, lightning in the atmosphere of Jupiter acts as a natural probe of cloud structure shedding light on the planet's rather complex atmospheric dynamics (Dyudina 2002). The article is divided as follows: in part I we discuss Galileo's observations and the details of its results. Part I is further divided into observations of lightning depth (1.1) and analysis (1.2). In part II we discuss the atmospheric physics and dynamics of Jupiter's storms and in part III present a discussion, all under the auspices of why the storms occur only in areas of cyclonic shear and near the centers of westward moving jets.

*first.surname@colorado

The Solid State Imager (SSI) detected the presence of 26 storms at 50° in both latitudes, with the northern hemisphere toting the most activity overall. The cells ranged in size of up to 1700 km. The greatest optical energy observed in a single flash was 1.6×10^{10} J, several times larger than terrestrial lightning. The average optical power per unit area is 3×10^{-7} W m^{-2}, comparable to the terrestrial value. The SSI observed jovian lightning on two successive orbits, at 93 and 16 to 19 jovian radii from the planets center, respectively. The area surveyed is approximately half the planets surface area.

Jupiters atmosphere, as observed in the 1979 Voyager space craft images, is distinguished by 12 zonal jet streams and approximately 80 vortices, the largest of which is the Great Red Spot (Marcus 2004). The thunderstorms occur in bright, zonal bands, expand rapidly and then pull apart in a few days by the surrounding shear flow. The spots nearly always occur in cyclonic shear zones, whereby rotation is clockwise in the southern hemisphere and counterclockwise in the north. The fact that lightning seems to assemble with a dark swath immediately west of the white cloud may be significant (Little *et al.* 1999).

Jovian lightning transpires in groups, typically separated by distances of 10,000 km. Table I displays a complete account of the storms observed by the probe. The storms are numbered one through 26, beginning at the highest northern latitude and progressing southward. The central latitudes of the storms are given in columns two and three. Column four identifies the images in which each storm was seen and is listed in chronological order. The line and sample numbers in columns five and six give the central point of each storm in each image. The seventh and eighth column provides the filter used. A clear filter is denoted CLR and spans 385 to 935 nm, RED spans 625 to 705 nm, GRN spans 520 to 600 nm, and VLT (violet) spans 385 to 430 nm. The wavelengths described are approximate (Klaasen *et al.* 1997). Column eight gives the exposure (in seconds), gain state, and mode. As lightning flash commonly lasts less than a second, and since storms have many flashes per second, the exposures recorded many flashes per storm. The gain state describes the cameras sensitivity representing values between one and four. The gain state ratio is inversely proportional to sensitivity and is 1.0, 4.824, 9.771, and 47.135, respectively (Klaasen *et al.* 1997). The final entry governs the camera mode of each image (two modes total) involving a 2×2 summation, in which the data numbers are summed and stored onto a tape recorder prior to being transmitted to Earth. Spacecraft attitude introduces an uncertainty of 20 to 40 pixels, depending on which mode the probe is committed to. An approximate estimate of the error in kilometers for a particular image, its resolution is multiplied by 20 for mode one and 40 for mode two. The distances resulting can therefore be further corrected by observation. Lightning at 47.5° latitude on the central meridian with 26 km per pixel resolution would be associated with an error of 20 pixels $\times$ 26 km / cos 47.5° = 770 km = 0.6° latitude (Little *et al.* 1999).

Myriad phenomena could inadvertently be mistaken for lightning. Those associated with Jupiter include auroras, satellites, fluxtube footprints, and meteors. Those associated with the camera include hot pixels and cosmic ray hits (Little *et al.* 1999). However, we are reasonably confident that the lightning listed in Table I is without error. Firstly, the easiest cases involve images in multiple frames, signifying that each storms location overall remained constant in each frame and the positions of each individual flash changed slightly. Cosmic ray hits exhibit a characteristic appearance, either a short tapered line or an isolated spot bereft of a skirt. Lightning, however, generally has a skirt. Meteors are usually so small that any one of them would be likely rejected along with cosmic ray hits.

The final column lists storm type. A subjective classification, it is mainly based on the storms appearance in an individual image. Type-one storms represent the largest, are elongated in the east-west direction, contain multiple flashes, and are normally associated with long exposures. Type-two storms are smaller, but contain multiple flashes. Type-three storms are smaller yet, whereas type-four storms are the smallest and dimmest of all observed. Some storms changed type, and the table reflects this observation. Hence a particular storms type classification may vary with camera settings and the deviations of individual flashes.

A "d" in Table I indicates that the storm appears to be a "double." Some doubles may be two flashes separated in position. The latitude, longitude, line sample, and size given for a "d"-type storm refer only to the larger member of the pair (Little *et al.* 1999). A typical storm separation is on the order of hundreds of kilometers.

The maximum east-west and north-south dimensions are provided in column nine. The dimensions were determined by the Galileo Team by counting the pixels and multiplying those numbers by the resolution in kilometers. The dimensions were then increased appropriately as needed in order to be made more suitable and to minimize errors.

Figure 1 displays the latitudes of the 26 storms with Jupiters zonal winds (Limaye 1986). Most of the 26 storms occur in cyclonic shear zones. The only exceptions are those storms between 40° and 50° north, which appear gathered near the center of westward moving jets. This region is the most disturbed region in Voyager movies, exhibiting small convective storms. The latter are where the absolute vorticity gradient reverses sign according to barotropic stability (Ingersoll *et al.* 1981, Limaye 1986). Table II (place table two here)

1.1 Depth of lightning

Light from jovian lightning penetrates the clouds, is scattered, and returns to Galileo information about about the lightning in addition to the shape, size, and opacity of the clouds. Dyudina *et al.* (2002) modeled a sample of six lightning storms retrieved from

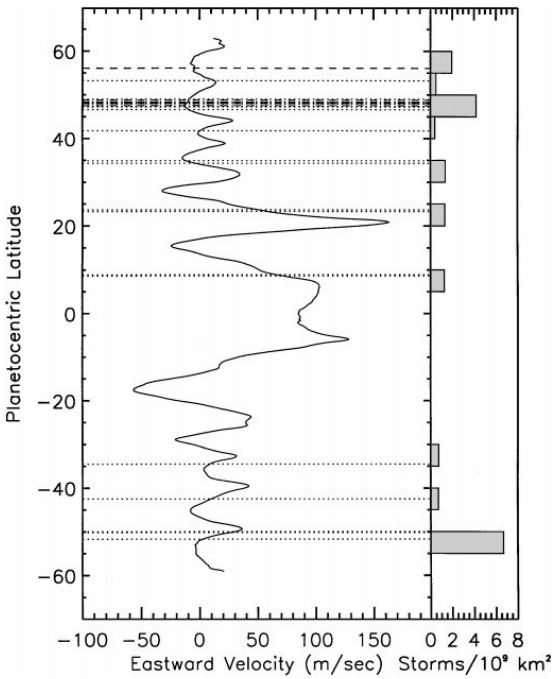

Figure 1: Latitudes of lightning storms in relation to the zonal winds. The wavy solid line shows the longitudinally averaged wind speed in 1979 (Limaye 1986). Those latitude intervals where this line slopes from upper left to lower right are cyclonic in the northern hemisphere, and are anticyclonic in the south. Latitude intervals where that line slopes from upper right to lower left are the opposite. The latitudes of the 26 storms from Table I appear as horizontal lines. The dotted lines are from the first orbit, while the dashed lines are from the second. A comparison of these lines with the velocity profile indicates that jovian lightning tends to occur within cyclonic shear zones and their poleward boundaries – westward moving jets.

the SSI to illuminate the depth, structure, and layering of the cloud deck by the criteria that (1) the brightness in the spot must not be saturated, (2) the spot not superimpose onto other lightning, and (3) the spot must be large, at least five to six pixels across. The model hastens the scattering of lightning-produced photons in a three-dimensional cloud. As only vertical lightning was modeled, facilitated by strong forward scattering (Tomasko *et al.* 1978), the Henyey-Greenstein function is

$$P(g_1, g_2, f, \theta) = f P_{HG}(g_1, \theta) + (1 - f)\ P_{HG}(g_2, \theta).$$

The two-terms are the Henyey-Greenstein function denoting forward and backward scattering lobes

$$P_{HG}(g,\theta) = \frac{1-g^2}{(1+g^2-2g\ \cos\theta)^{3/2}},$$

where θ is the scattering angle, f is the fraction of forward versus backward scattering, g_1 is positive and displays the sharpness of the forward scattering lobe, and g_2 is negative and displays the sharpness of the backscattering lobe. The parameters g_1, g_2, and f are derived by Tomasko *et al.* (1978) from the Pioneer 10 images. They use g_1 = 0.8, g_2 = -.075, and f = 0.954. The model shows that the cloud depths for the six storms based on Monte Carlo methods range in depth from 35 to 171 km (*see Table 2*). The smallest uncertainty is 30 km (flash three) and the largest is 97 km (flash four). Three acceptable models were used as column six indicates in the pressure-temperature profiles.

TABLE II
Derived Depth of the Lightning Below the Cloud Tops for Different Flashes

	HWHM (km)	Emission angle	Depth/HWHM	Lightning depth (km)	Acceptable models (br. fallof shape)	Acceptable models (az. asymmetry)
Flash 1	87	55.7°	1.1–1.6	95–140	3D clouds	3D clouds
Flash 2	69	69.1°	1–2.3	68–158	Plane-parallel or 3D	3D clouds
Flash 3	37	56.6°	0.9–2.1	35–79	Plane-parallel or 3D	3D clouds
Flash 4	72	57.0°	1–2.4	74–171	Plane-parallel or 3D	3D clouds
Flash 5	42	50.6°	1.1–2.1	47–90	Plane-parallel clouds	Plane-parallel clouds
Flash 6	50	50.6°	1–2.2	52–110	Plane-parallel or 3D	3D clouds

Note. Emissiona angle is measured with respect to the local vertical. The Depth/HWHM ratio in the fourth column is measured in the coarse resampled grid, which corresponds to the resolution of each flash. Note that the Depth/HWHM ratio in the fourth column is obtained from Fig. 9 by considering the range of acceptable models, i.e., choosing between the curves for standard plane-parallel, standard plane-parallel with Rayleigh scattering, and Hemispheric+haze models. The choice is made according to the sixth column of the table. The range of the values for the chosen curves and for different optical depths is then divided by the correction coefficient from Fig. 11. The coefficient is taken at the appropriate resolution, i.e., at the HWHM (pixels) appropriate for each of the six flashes.

The results reflect graphically the tabulated values. The data for the six flashes show diffuse, scattered light. Therefore, clouds above the lightning may be opaque enough to block direct light (Dyudina 2002). The models indicate that the only clouds with optical depths of more than five can block direct light and produce a fine brightness distribution. Additionally, optically thick clouds above lightning may reflect most of the energy back downward. If the atmospheric absorption is weak, the Rayleigh scattering atmosphere will reflect most of the energy back upward. In the absence of scattering, the absorption of parallel beam radiation traversing downward through a horizontal layer of gas of infinitesimal thickness dz is proporional to the number of molecules per unit areas that are absorbing radiation along the path (Wallace 1977). This relationship, derived by Wallace (1977), is expressed in the form

$$da_\lambda \equiv -\frac{dE_\lambda}{E_\lambda} = -k_\lambda \rho \sec\phi dz,$$

where ρ is the gas density and ϕ the zenith angle. Here absorbed monochromatic irradiance is expressed as an incremental amount of depletion of the incident beam. The fraction of parallel beam radiation that is scattered when traversing downward through a layer of infinitesimal thickness is

$$ds_\lambda \equiv \frac{dE_\lambda}{E_\lambda} = KA \sec \phi dz,$$

where K is a dimensionless coefficient, and A is the cross-sectional area that the particles in a unit volume present to the beam of incident radiation (Wallace 1977). The model does not attempt to separate gaseous absorption and absorption in the cloud particles. Realistically, clouds may have a breadth of transmissions. No effective attenuation may also be possible (transmission unity). Cloud transmission is important for estimating total lightning and thunderstorm energy (Borucki *et al.* 1982, Borucki and Magalhaes 1992, Little *et al.* 1999).

Ingersoll (2000) alternatively determined (based on the inferred abundance of water in the deep atmosphere assuming the abundance ratios of oxygen to hydrogen, carbon to hydrogen, nitrogen to hydrogen, and sulfur to hydrogen are three times those in the Sun (Niemann 1998, Folkner 1998)) that the base of the water cloud is at approximately 80 km, with water the principal agent of cloud electrification, as the other condensates are thought to be less abundant at that altitude (Gibbard *et al.* 1995, Yair *et al.* 1995).

Important factors contributing to the robustness of the model include the Rayleigh scattering from the atmosphere below the clouds of five to 20 bars. Laboratory experiments by Borucki *et al.* (1996) proposed that most of the lightning energy of the Galileo clear filter is expected to emit around 650 to 680 nm and 480 to 500 nm bands. This implies that optical depth for Rayleigh scattering is reached at approximately 20 bars for the former range and seven bars for the latter range (Dyudina 2002). The main atmospheric absorber for the mentioned wavelengths is methane (Karkoschka *et al.* 1994). The methane is small in the upper atmosphere. At five to 20 bars, pressure and temperature may enhance the absorption such that the atmosphere below the clouds would be effectively black as was assumed on the standard Dyudina model.

But a sense of uncertainty looms over the approximations and assumptions due to a poor understanding of the exact locations of water, NH_4SH, and ammonia cloud layers. The stratified layers are reasonably assumed to be at their respective equilibrium condensation levels (Weidenschilling and Lewis 1973). Yet, the dynamics may be too complicated and too chaotic to apply a one size-fits-all approach to the vertical distribution of a trace species. The myriad colors of its fluid medium sinuating in the atmosphere indicate chemical disequilibrium and may signify that the constituents situated at their theoretical equilibrium condensation levels may be wishful thinking, but the approximation provides physical insight and a place-holder to modify the models.

1.2 Analysis of lightning

The largest individual flash observed by Galileo is 1.5×10^9 J. To estimate the planets optical power per unit area, Little *et al.* (1999) took the average power per storm, and multiplied by the number of storms per unit area. Twenty-six storms were referenced, and the total area surveyed was 39.5×10^9 km^2. Thus the power per unit area is 0.30 $\times 10^{-6}$ W m^{-2}. Borucki *et al.* (1982) estimated $2.5 \pm 1.9 \times 10^9$ J per flash and an average rate of 4×10^{-3} flashes per km^2 per year, or 0.32×10^{-6} W m^{-2}.

A lower bound on the flash rate (flashes per unit time) can be obtained by taking the average of the 12 observed flashes (in the scanned frame of 36 flashes per three storms that Little *et al.* (1999) analyzed, for example), multiplying by 26 storms (refer to Table I), dividing by the 59.8 second exposure time, and then dividing by the total area surveyed (39.5×10^9 km^2). The result is 4.2×10^{-3} flash per km^2 per year. This value is 1000 times smaller than the terrestrial rate of six flashes per km^2 per year (Borucki and Chameides 1984, Uman 1987).

Terrestrial lightning and jovian lightning are thus similar in some respects – the energy in the largest flashes and the optical power per unit area – but different in others. Earth and Jupiter diverge form one another in their global flash rates, but that could be attributed to the greater dynamic range of terrestrial lightning observations compared with that of Galileo (Borucki and Chameides 1984).

The spatial distribution of lightning invokes curiosity. The SSI confirmed the latitude zone between 45° and 50° in the north of having more lightning per unit area. The same seems to be true of the latitude zone from -50° to -55° in the south, and the incidence of lightning seems to exhibit a general pole-ward trend in both hemispheres. The trends are not currently understood, but may be due to an increase heat flux from the planetary interior at high latitudes (Ingersoll and Porco 1978, Pirraglia 1984). The probes data conclusively suggests that the northern hemisphere has more lightning than the southern hemisphere. This asymmetry has yet to be explained. Perhaps future modeling can assist in understanding these patterns and illuminate the confused jumble of atmospheric dynamics on Jupiter.

2 Atmospheric physics and dynamics

Jupiter's dominant, macro-scale weather patterns are zonal jets and long-enduring ovals. The jets have been flowing east and west at constant speeds of up to 180 m s^{-1} for over 100 years (Ingersoll *et al.* 1981, Limaye 1986, Vasavada *et al.* 1998). They are on the receptive end of micro-scale eddies, pumping eastward momentum into westward moving jets. This momentum transfer was predicted by numerical models before it was observed on Jupiter (Williams 1978). The large ovals swing between the jets in an anti-cyclonic direction clockwise in the northern hemisphere and counterclockwise

in the southern hemisphere, where they frequently incorporate small anticyclonic eddies (Mac Low and Ingersoll 1986, Dowling and Ingersoll 1989). Ingersoll *et al.* (2000) proposed that that eddies ultimately drive both the jets and ovals and receive their energy from moist convection. This concept underlies observations of lightning on Jupiter (Gibbard *et al.* 1995, Yair *et al.* 1995) and is the main focus of part II of this article. This also explains the anticyclonic rotation and poleward drift of eddies, and implies patterns of upwelling and down-welling that resemble patterns of large-scale convection in Earth's atmosphere.

Jupiter is divided into dark and bright bands, namely belts and zones that envelop the planet at constant latitude. The darker belts have a disturbed, chaotic appearance, whereas the lighter zones are more uniform. The zonal jets are located on the boundaries between the belts and zones, with the westward moving jets on the poleward edges of belts and the eastward jets on the poleward edge of zones (Ingersoll *et al.* 2000). Thus the belts are cyclonic, and the zones, anti-cyclonic.

The Galileo probe indicates that the lightning occurs mainly within belts, and is associated with the optically thick, high white cloud groups that appear instantaneously and grow to have diameters on the order of 1000 km in a matter of days (Little *et al.* 1999, Banfield *et al.* 1998, Gierasch *et al.* 2000). Current research and modeling suggest that the tops of the groups are at pressures of a few hundred millibar, where ammonia, H_2S, and water are possible condensates. Near the clusters are clouds at pressures greater than three bar, where water is the only condensable (Banfield *et al* 1998, Gierasch *et al.* 2000). Water is thought to be the principal constituent at altitudes of 80 km where Ingersoll (2000) speculated a cloud deck may persist.

It is argued that the belts have a net rising motion at the cloud base, as lightning implies moist convection (Salby 1996) requiring an ample quarry of moisture-laden air from Jupiters interior. Other observations imply the opposite (Gierasch *et al.* 1986, West *et al.* 1986, Ingersoll 1995) (rising in the zones and sinking in the belts) in so far as describing the dynamics at cloud-top layers. Comparably, both theories imply that in a belt two vertical currents converge within a cloud. Vertical convergence must be balanced by horizontal divergence, resulting in a flow within the clouds from belts to zones (Ingersoll 2000).

On Jupiter, the high, thick clouds of the convective groups exist alongside some of the clearest regions on the planet, namely the "hot spots." The convective clouds penetrate higher than the average cloud top, and the hot spots continue deeper than the water cloud base. This mixing of processes gives the belts their disturbed, chaotic, appearance. Averaged over the entire belt, the next effect is upwelling at the base of the clouds and downwelling at the tops, according to current interpretations.

If we assume that eddies are moist convective structures, then we have a self-regulating cycle. The eddies maintain the jets, and the interaction produces a pattern of upwelling and downwelling that assists to maintain the eddies. There is no violation

of thermodynamics (Ingersoll *et al.* 2000) as the eddies maintain a separate source of energy. Two-dimensional turbulent flows have dynamical constraints not found in three-dimensional flows. In two dimensions, vortices grow by amalgamating, and on a rotating planet they amalgamate into cyclonic and anticyclonic bands (Williams 1978, Rhines 1975, Maltrud *et al.* 1991, Panetta 1993, Cho and Polvani, 1996, Huang and Robinson 1998).

Other properties of the eddies are consistent with moist convection. The region northwest of the Great Red Spot is a primary example as the eddies there are rather large and easier to cope with visually.

This region is exemplary in the sense that it is where lightning is seen in bright white cloud clusters (Gierasch *et al.* 2000). These groups emerge suddenly and grow swiftly, and are destroyed in the cyclonic shear or drift poleward and assume stable, anticyclonic, activity while progressing west with the current on the southern edge of the South Equatorial Belt (SEB) (Mac Low and Ingersoll 1986). They then confront the Great Red Spot (GRS) after rounding the planet and generally merge into it. Thus, eddies in the SEB emerge as moist convective structures complete with lightning, and disintegrate principally by giving their energy either to the SEB or to the GRS.

As indicated by Borucki and Williams (1986), the apparent size of a lightning flash at the top of Jupiter's clouds is a measure of the depth of the light source. Deeper flashes appear broader as their light undergoes more scattering by cloud particles. Jupiters atmosphere is thought to contain three major cloud decks above the eight-bar level and two aerosol layers above these clouds. The upper cloud is composed of ammonia, the middle consists mainly of NH_4HS, and the lower cloud deck has been argued to be water. It was found that the flashes appear to originate at the five-bar level as mentioned above, therefore inferring that lightning occurs in the water cloud.

These results are striking in lieu of the fact that lightning is invariably associated also with bright dayside clouds that seem to be much higher than water clouds. It may be that these bright clouds are simply proxies of a deep process, created themselves by updrafts that originate at much lower levels. As stressed earlier, jovian lightning may occur mainly inside the deep roots of such clouds. Figure 3 shows a current that originates west of the storm and flows to the west. Flow divergence exists near the origin of the current. Ingersoll (2002) estimated that the divergence over an area 1000 km $\times$ 1000 km is 20 km^2 s^{-1}. In order to supply this fluid, upwelling from below is required as the overlying region is stably stratified and would not be expected to decent. Another feature of the local flow near the storm is the occurrence of vorticity of both signs, as mentioned above, indicating that both cyclonic and anticyclonic eddies are being generated by the storm.

Assuming storm homogeneity, an estimate of the total heat flux can be given. Previous estimates suggest that moist convection might carry significant flux. The temperature excess in convective updrafts in intense storms on Jupiter has been estimated

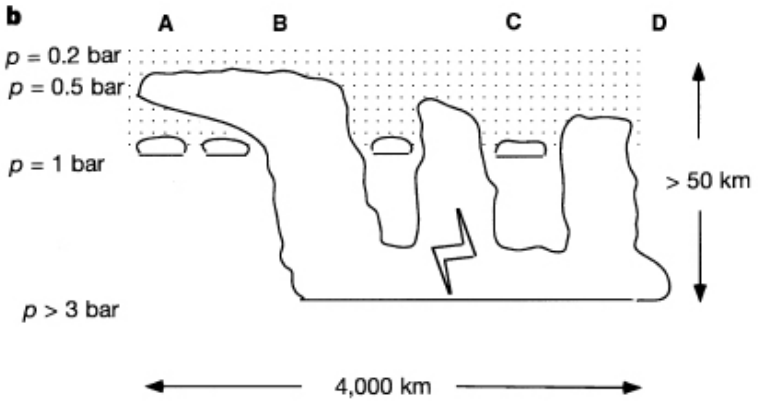

Figure 2: Expanded view of storm with colour coding to bring out deep cloud in red, and sketch of storm structure. a, Image: the continuum is in red, and the weak methane band is in green and blue. White regions are higher cloud, red regions are deeper cloud. b, Sketch: dotted regions show haze. Cloud outlines show optically thick cloud with opacity of at least 5 to 10 optical depths, caused by to condensation of water at the deepest levels and possibly a combination of water, ammonia and ammonium hydrogen sulphide at shallower levels10. The southeastern corner (D) is particularly dark in the methane band. It is plotted well by models that contain the two high haze layers plus an optically thick cloud at a pressure level (p) of 3 bar or greater, and no sheet cloud at 0.9 bar. This is indicated in the schematic by a small foot extending from the right hand edge of the deepest cloud. Across the central portion of the storm, high brightness in the continuum requires a deep cloud, but analysis of local brightness variations shows that there is also a spatially variable cloud near 0.9 bar. Finally, analysis of the bright spots (A) just northwest of the storm shows that optically thick cloud has penetrated up to at least the 0.5-bar pressure level. Analysis of spatial variations in brightness suggests that the deep cloud, visible in the continuum, is more spatially homogeneous than the upper clouds. This sketch is meant only to illustrate heights schematically. In particular, where thick cloud pushes to high elevations, the sketch indicates a solid tall tower of cloud, but in fact the data gives no information beneath the highest optically thick surface. In addition, cloud bases might be even deeper than indicated.

from cloud height to be roughly five K, assuming that the fluid ascends until it reaches its level of neutral buoyancy (Banfield *et al.* 1998). A 1000 km $\times$ 1000 km area implies a total power carried by sensible heat of about 5×10^{15} W. The number of lightning storms discovered by the probe in 1997 was 0.66×10^{-9} per km^2 (Little *et al.* 1999). Multiplying this by the power per storm gives an average heat flux of 3.3 W m^{-2}. Jupiter's internal heat flux, averaged over its surface, is then approximately 5.7 W m^{-2}. The true depth of the outflow is not known. Nonetheless, it may be that moist convective storms carry a large portion of the heat flux through an atmospheric layer between pressures of several bars to less than one.

The association of lightning with cyclonic regions is important as it is may allude to the mechanics of moist convection as a dominant mode of vertical heat transfer and illuminate the coupling of thunderstorms to westward moving jets and cyclonic shear. These storms appear to be comparable to groups of storms cells on Earth, namely convective complexes (Maddox 1980, Emanuel 1994, Houze 1993).

The energy source driving Jupiters active meterology is not well understood (Gierasch *et al.* 2000). However, we can approximate the atmospheric dynamics of Jupiter if we assume that the physics of storm formation is comparable to thunderstorm formation

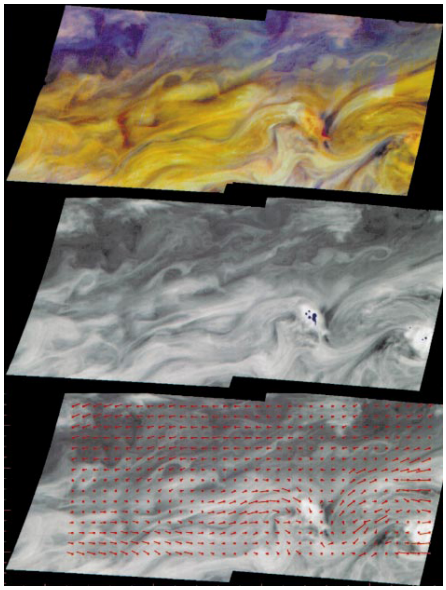

Figure 3: Mapped images of the storm region. There are two storm centres, near latitude 14° S, longitude 268° W and latitude 15° S, longitude 263° W, respectively. Detailed analysis has been carried out only for the left (west) storm. a, Colour images in a strong methane band (889 nm, blue), in a less strong methane band (727 nm, green), and at a continuum wavelength with negligible gas absorption (756 nm, red) are superposed. Sunlight penetrates to about the 0.5 bar level in the strong methane band and to 3 bar in the weak methane band, but the continuum penetrates more deeply. A cloud that is visible in the continuum but not in the methane band images is thus at a pressure greater than 3 bar. In practice, radiative transfer models are used to and cloud structure in local regions, following a procedure described elsewhere. The strongly red feature on the southeastern corner of the storm near 268° W, 14° S is unusually dark in both methane bands and represents deep cloud. b, Night-side images in blue are superposed on a day-side continuum image, showing points where lightning appears in the night-side images. c, Map of velocity vectors. Latitudes are planetocentric. The longest vector represents 70 m s^{-1}. Markers point downwind from the grid points. A large-scale current is from west to east near the north edge of the domain, and opposite near the south edge of the domain, consistent with previous measurements of Jupiter's atmospheric jets. The region between these currents has cyclonic vorticity. Local flow near the storms is complex. The flow loop at 265° W, 14° S, just to the east of the storm, shows counterclockwise rotation, corresponding to local anticyclonic vorticity. In contrast, there is strong cyclonic shear at 269° W, 13° S, just to the northwest of the storm. .

on Earth, if terrestrial processes are ignorantly assumed.

According to Holton (1992), the development of a thunderstorm shows a tendency to facilitate a rotating mesocyclone from an intially nonrotating environment. The dominance of cyclonic rotation is such systems suggest the importance of a Coriolis force in supercell dynamics. However, though not derived here, the rotation of a planet is not relevant to the development of rotation in thunderstorms. The Euler momentum equation using the vector identity

$$(\mathbf{U}\cdot\nabla)\mathbf{U} = \nabla\left(\frac{\mathbf{U}\cdot\mathbf{U}}{2}\right) - \mathbf{U}\times(\nabla\times\mathbf{U})$$

to obtain

$$\frac{\partial\mathbf{U}}{\partial t} = -\nabla\left(\frac{p}{\rho_0} + \frac{\mathbf{U}\cdot\mathbf{U}}{2}\right) + \mathbf{U}\times\omega + b\mathbf{k}. \tag{1}$$

Taking $\nabla\times$ eq. 1 and recalling that the curl of the gradient vanishes, we obtain the three-dimensional vorcity equation

$$\frac{\partial \omega}{\partial t} = \nabla\times(\mathbf{U}\times\omega) + \nabla\times(b\mathbf{k}). \tag{2}$$

Letting $\sigma = \mathbf{k}\cdot\omega$ be the vertical component of vorticity and taking the dot product of $\mathbf{k}$ and eq. 2, we obtain an equation for the tendency of σ in a nonrotating reference frame:

$$\frac{\partial \sigma}{\partial t} = \mathbf{k}\cdot\nabla\times(\mathbf{U}\times\omega). \tag{3}$$

Bouyancy affects only the horizontal vorticity components. We now consider a flow consisting of a single convective updraft in a basic state westerly flow that depends entirely on z . We let

$$\omega = \mathbf{j}\frac{d\bar{u}}{dz} + \omega'(x,y,z,t),$$
$$\mathbf{U} = \mathbf{i}\bar{u} + \mathbf{U}'(x,y,z,t)$$

and considering that the form of the right handside in eq. 3 becomes

$$\mathbf{k}\cdot\nabla\times(\mathbf{U}\times\omega) = -\mathbf{k}\cdot\nabla\times\left(\mathbf{i}w'\,\frac{d\bar{u}}{dz} + \mathbf{j}\bar{u}\sigma'\right).$$

We find the vorticity tendency is

$$\frac{\partial \sigma}{\partial t} = -\bar{u}\,\frac{\partial \sigma'}{\partial x} + \frac{\partial w'}{\partial y}\,\frac{\partial \bar{u}}{\partial z}. \tag{4}$$

The first term on the right in eq. 4 is the advection by the basic state flow. The second term represents tilting of horizontal shear vorticity into the vertical by differential vertical motion. Since $d\bar{u}/dz$ is positive, the vorticity tendency owing to its tilting will be positive to the south of the updraft core and negative to the north of the updraft core. Consequently, a counterrotating vortex pair is established with cyclonic rotation to the south and anticyclonic rotation to the north of the initial updraft. Holton (1992) suggests that to understand the generation of updrafts in the vortices on the peripheries of the storm we examine the perturbation pressure field. An equation for the disturbance pressure is obtained by taking the dot product of ∇ and eq. 1 to yield

$$\nabla^2\left(\frac{p}{p_0}\right) = -\nabla^2\left(\frac{\mathbf{U}\cdot\mathbf{U}}{2}\right) + \nabla\cdot(\mathbf{U}\times\omega) + \frac{\partial b}{\partial z}. \tag{5}$$

The first two terms on the right of eq. 5 represent dynamical forcing, while the last term represents buoyancy forcing. Observations and numerical models suggest the buoyancy forcing in eq. 5 produces pressure perturbations that tend to accommodate

the buoyancy force in the vertical momentum equation. Dynamically forced pressure perturbations, alternatively, may generate substantial vertical accelerations.

In order to compute the dynamical contribution to the disturbance pressure gradient force in either the right of left side vortex, Holton (1992) uses cylindrical coordinates (r, λ, z) centered on the axis of rotation of either vortex and assumes to a general approximation the asimuthal velocity v_λ (positive for cyclonic flow) is independent of λ. The storm's relative horizontal motion and vertical component of vorticity are given conditionally by

$$\mathbf{U}' \approx \mathbf{j}_\lambda v_\lambda,$$

$$\mathbf{k} \cdot \omega' = \sigma' \approx \frac{1}{r} \frac{\partial (r v_\lambda)}{\partial r},$$

where $\mathbf{j}_\lambda$ is the unit vector in the azimuthal direction (positive counterclockwise), and r is the distance from the axis of the vortex. Letting $\mathbf{i}_\lambda$ be the unit vector in the radial direction we have

$$\mathbf{U} \times \omega \approx \mathbf{i}_\lambda \frac{v_\lambda}{r} \frac{\partial (r v_\lambda)}{\partial r}.$$

Assuming that the vertical scale is considerably large than the radial scale, the Laplacian in cylindrical coordinates can be approximated by

$$\nabla^2 \approx \frac{1}{r} \frac{\partial}{\partial r} \left(r \frac{\partial}{\partial r} \right).$$

From eq. 5 the dynamical component of the pressure perturbation in the vortices (p_d) can be expressed as

$$\frac{1}{r} \frac{\partial}{\partial r} \left(\frac{r}{\rho_0} \frac{\partial p_d}{\partial r} \right) \approx -\frac{1}{r} \frac{\partial}{\partial r} \left[r \frac{\partial (v_\lambda^2/2)}{\partial r} \right] + \frac{1}{r} \frac{\partial}{\partial r} \left[v_\lambda \frac{\partial (r v_\lambda)}{\partial r} \right] = \frac{1}{r} \frac{\partial v_\lambda^2}{\partial r}. \tag{6}$$

Integrating eq. 6 with respect to r, Holton (1992) obtains the equation of cyclostrophic balance

$$\frac{1}{\rho} \frac{\partial p_d}{\partial r} \approx \frac{v_\lambda^2}{r}, \tag{7}$$

where cyclostrophic balance occurs when the horizontal pressure gradient and centrifugal forces exert equally in opposite directions. Thus, there is a pressure minimum at the vortex center irrespective of whether the rotation is cyclonic or anticyclonic. A "centrifugal pump" arises due to the vortex twisting and stretching effectively causing a negative dynamical pressure perturbation centered in the vortices. This produces an upward-directed dynamical contribution to the vertical component of the pressure gradient force and thus provides an upward acceleration, producing updrafts in the cores of the vortices. For small vertical accelerations, this would amply apply to a jovian scenario.

As mentioned earlier, the tilting and stretching of horizontal vorticity concerning the vertical shear of the basic state wind can account for the mesoscale rotating supercells. Numerical simulations suggest that these tend, rather, to involve tilting and stretching of especially strong horizontal vorticity produced by horizontal gradients in buoyancy that occur near the surface where negatively buoyant updrafts produced by convective downdrafts meet moist, warm, boundary layer air. Jovian storms are typically a few

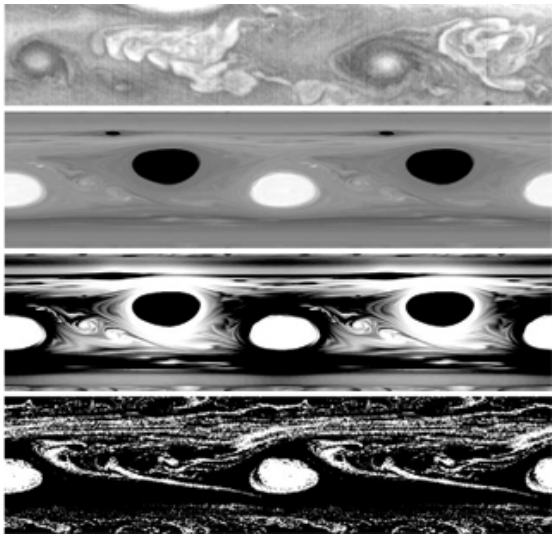

Figure 4: Observed and simulated jovian clouds. a, Voyager mosaic showing 2 of the 12 cyclone/anticyclone pairs at 418° S. The clouds of cyclones are large, tangled and filamentary, whereas those of anticyclones are bright, 2:1 ovals surrounded by dark rings. b, Simulated potential vorticity q, with cyclonic q shown black and anticyclonic q white. c, q of the same flow in b with cyclonic (q , 0) shown black and anticyclonic q white. d, Simulated clouds of the flow in b, where white pixels represent NH_3 ice. For anticyclones: ice is created in the vortex interior where q . 0 and there is weak upwelling; ice is rapidly melted in the ring around the vortex where q , 0; the clouds are ovals (coincident with regions where q . 0) surrounded by dark rings (coincident with q , 0). For cyclones: turbulence spreads and twists the clouds created at the peripheral rings (where q . 0); the turbulence fills the interiors (where q , 0) with cloud filaments before they melt.

hundred km in diameter but it is not uncommon to observe one as large as 1000 km. The life-span is on the order of a half-day and sometimes a few days (Houze 1993). They tend to form where the vertical shear in the mean wind is small. The jovian case are observed near zero in the mean zonal wind profile, which may also correspond to weak vertical shear. Mesoscale convective complexes are usually associated with cyclonic low-level winds, large-scale ascent at mid-tropospheric levels, and anticyclonic circulation. They are accompanied by heavy precipitation. They occur over oceans at low latitudes and over midlatitude continental regions in the summer. The convective complexes form by large-scale waves with air mass contrasts (Ingersoll 2000). These striking similarities suggest that if the analog with jovian storms is correct, then large-scale convergence exists at low levels beneath the storm, where moisture resides. Nevertheless, it seems

likely that lightning does not occur at random across the jovian disk (West *et al.* 1986).

3 Discussion

A remaining uncertainty concerns what circulation is like below the surface. Because deep observations are presently impossible, a strong sense of understanding of why precisely thunderstorms form near cyclonic flow and within the centers of westward moving jets is of current, pressing concern. Busse (1976) proposed a model that was partly theoretical and partly empirical. He claimed that Jupiters internal flow in the presence of a rapid rotation in an internal heat source would yield a form of concentric cylindrical shells aligned with the planets spin axis. Each shell contains cylindrical vortices, having the same diameter as the shell thickness, which transport heat to the surface. According to this model, belts and zones appear where the shells intersect the surface, and disappear at latitudes above 45° because the solid planet interior limits the radius of the innermost shell (Seiff 2000).

The observations of lightning discharges in the jovian atmosphere were attributed to convective activity in the water cloud region of the troposphere (Yair *et al.* 1995). Results from various numerical models of a convective cloud show that these are large cumulonimbus clouds, with vertical dimensions at times greater that 40 km and sustained interior pressures of over 3 bars. A study showed that the minimum water abundance in Jupiters atmosphere, whereby convective clouds can separate enough charge to induce critical electrical fields, is 0.5 times the solar value (Yair *et al.* 1995). Assuming that lightning transpires wherever the breakdown value of the electric field is exceeded, we find that jovian water clouds can easily produce many lightning flashes. The full description of jovian atmospheric dynamics is currently complex; granted if new probing measures to investigate deeper in the atmosphere is developed in the near future (may become even more complex), researchers will have to contend with and depend entirely on surface process-modeling to elucidate the chaotic and yet rich undulations of Jupiters fluid medium.

Acknowledgements. This paper was motivated by a chapter I read in The New Solar System by Andrew Ingersoll discussing the atmospheric physics of Jupiter's fluid medium, with a reference to the planet's rather ordered thunderstorm locations. The topic presented itself at the right moment and so has been studied to the best that time and resources permit (by undergraduate standards in particular). Additional motivation was provided by the instructor, professor Esposito, for encouraging me instantly to pursue it the moment I mentioned in class. Thanks to Dr. Ingersoll for his immediate reply when I was frantically searching for appropriate articles he authored.

References

[1] Banfield, D., P. J. Gierasch, M. Bell, E. Ustinov, A. P. Ingersoll, A. R. Vasavada, R. A. West, and M. J. S. Belton 1998. Jupiter's cloud structure from Galileo imaging data. *Icarus* **135**.

[2] Bar-Nun, A. 1975. Thunderstorms on Jupiter. *Icarus* **24**.

[3] Bar-Nun, A., and M. Podolak 1985. The contribution by thunderstorms to the abundances of CO, C_2H_2, and HCN on Jupiter. *Icarus* **64**.

[4] Borucki, W. J., A. Bar-Nun, F. L. Scarf, A. F. Cook II, and G. E. Hunt 1982. Lightning activity on Jupiter. *Icarus* **52**.

[5] Borucki, W. J., and W. L. Chameides 1984. Lightning: Estimates of the rates of energy dissipation and nitrogen fixation. *Rev. Geophys. Space Phys.* **22**.

[6] Borucki, W. J., and M. A. Williams 1986. Lightning in the jovian water cloud. *J. Geophys. Res.* **91**.

[7] Borucki, W. J., and J. A. Magalhaes 1992. Analysis of Voyager 2 images of jovian lightning. *Icarus* **96**.

[8] Borucki, W. J., C. P. McKay, D. Jebens, H. S. Lakkaraju, and C. T. Vanajakshi 1996. Spectral irradiance measurements of simulated lightning in planetary atmospheres. *Icarus* **123**.

[9] Busse, F.H. 1976. A simple model of convection in the Jovian atmosphere. *Icarus* **29**.

[10] Cho, J. Y. -K. & Polvani, L. M. The morphogenesis of bands and zonal winds in the atmospheres on the giant outer planets. *Science* **273** (1996).

[11] Dowling, T. E. & Ingersoll, A. P. Jupiter's Great Red Spot as a shallow water system. *J. Atmos. Sci.* **46** (1989).

[12] Dyudina, U.A., A.P., Ingersoll, A. R. Vasavada, S. P. Ewald Galileo SSI Team. Monte Carlo Radiative Transfer Modeling of Lightning Observed in Galileo Images of Jupiter, *Icarus* **160** (2002).

[13] Folkner, W. M., Woo, R. & Nandi, S. Ammonia abundance in Jupiter's atmosphere derived from theattenuation of the Galileo probe's radio signal. *J. Geophys. Res.* **103** (1998).

[14] Gibbard, S., E. H. Levy, and J. I. Lunine 1995. Generation of lightning in Jupiters water cloud. *Nature* **378**.

[15] Gierasch 1981. Thermal structure and dynamics of the jovian atmosphere. I. The Great Red Spot. *J. Geophys. Res.* **86**.

[16] Gierasch, P. J., B. J. Conrath, and J. A. Magalhães 1986. Zonal mean properties of Jupiters upper troposphere from Voyager infrared observations. *Icarus* **67**.

[17] Gierasch, P.J. Ingersoll, A.P. Banfield, Ewald, S.P. Helfenstein, P. Simon-Miller, Vasavada, A. Breneman, H.H. Senske, D.A., and the Galileo Imaging Team. 2000. Observations of moist convection in Jupiter's atmosphere. *Nature* **403**.

[18] Golde, R. H. (Ed.) 1977. Lightning, 906 pp., Academic Press, New York

[19] Holton, J. R. An Introduction to Dynamic Meteorology, 511 pp., 3rd ed. (Academic, San Diego, 1992).

[20] Huang, H.P. & Robinson, W. A. Two-dimensional turbulence and persistent zonal jets in a global barotropic model. *J. Atmos. Sci.* **55** (1998).

[21] Hunt, G. E., Müller, J. P. & Gee, P. Convective growth rates of equatorial features in the Jovian atmosphere. *Nature* **295** (1982).

[22] Ingersoll, A. P., and C. C. Porco 1978. Solar heating and internal heat flow on Jupiter. *Icarus* **35**.

[23] Ingersoll, A. P., R. F. Beebe, J. L. Mitchell, G.W. Garneau, G. M. Yagi, and J.-P. Müller 1981. Interaction of eddies and mean zonal flow on Jupiter as inferred from Voyager 1 and 2 images. *J. Geophys. Res.* **86**.

[24] Ingersoll, A. P., A. R. Vasavada, B. Little, C. D. Anger, S. J. Bolton, C. Alexander, K. P. Klaasen, W. K. Tobiska, and the Galileo SSI Team 1998. Imaging Jupiters aurora at visible wavelengths. *Icarus* **135**.

[25] Ingersoll, A. P., Gierasch, P. J., Banfeld, D., Vasavada, A. R. and the Galileo Imaging Team. Moist convection as an energy source for the large-scale motions in Jupiter's atmosphere. *Nature* **403** (2000).

[26] Karkoschka, E. 1994. Spectroscopy of the jovian planets and Titan at 300 to 1000 nm wavelength: The methane spectrum. *Icarus* **111**.

[27] Klassen K. P., M. J. S. Belton, H. H. Breneman, A. S. McEwen, M. E. Davies, R. J. Sullivan, C. R. Chapman, G. Neukum, C. M. Heffernan, A. P. Harch, J. M. Kaufman, W. J. Merline, L. R. Gaddis, W. F. Cunningham, P. Helfenstein, and T. R. Colvin 1997. Inflight performance characteristics, calibration, and utilization of the Galileo solid-state imaging camera. *Opt. Eng.* **36**.

[28] Limaye, S. S. 1986. Jupiter: New estimates of the mean zonal flow at the cloud level. *Icarus* **65**.

[29] Mac Low, M.-M., and A. P. Ingersoll 1986. Merging of vortices in the atmosphere of Jupiter: An analysis of Voyager images. *Icarus* **65**.

[30] Maddox, R. A. Mesoscale convective complexes. *Bull. Am. Meteorol. Soc* **61** (1980).

[31] Emanuel, K. A. Atmospheric Convection (Oxford Univ. Press, New York, 1994).

[32] Houze, R. A. Cloud Dynamics (Academic Press, San Diego, 1993).

[33] Little, B. et al. Galileo images of lightning on Jupiter. *Icarus* **142** (1999).

[34] Magalhães, J. A., and W. J. Borucki 1991. Spatial distribution of visible lightning on Jupiter. *Nature* **349**.

[35] Maltrud, M. E. & Vallis, G. K. Energy spectra and coherent structures in forced two-dimensional and beta-plane turbulence. *J. Fluid Mech.* **228**, (1991).

[36] Marcus, P.S., Kundu, T., Lee, Changhoon Source. 2000. Vortex dynamics and zonal flows. *Physics of Plasmas* **7** 5 pt 2, May, 2000.

[37] Niemann, H. B., S. K. Atreya, G. R. Carignan, T. M. Donahue, J. A. Haberman, D. N. Harpold, R. E. Hartle, D. M. Hunten, W. T. Kaspzrak, P. R. Mahaffy, T. C. Owen, and S. H. Way 1998. The composition of the jovian atmosphere as determined by the Galileo probe mass spectrometer. *J. Geophys. Res.* 103.

[38] Panetta, R. L. Zonal jets in wide baroclinically unstable regions: Persistence and scale selection. *J. Atmos. Sci.* **50** (1993).

[39] Pirraglia, J. A. 1984. Meridional energy balance of Jupiter. *Icarus* **59**.

[40] Salby, M. L. 1996. Fundamentals of Atmospheric Physics. Academic Press, San Diego.

[41] Seiff, A. 2000. Dynamics of Jupiter's atmosphere. *Nature* **403**.

[42] Tomasko, M. G., R. A.West, and N. D. Castillo 1978. Photometry and polarimetry of Jupiter at large phase angles. I. Analysis of imaging data of a prominent belt and a zone from Pioneer 10. *Icarus* **33**.

[43] Uman, M. A. 1987. The Lightning Discharge. Academic Press, New York.

[44] Vasavada, A. R., A. P. Ingersoll, D. Banfield, M. Bell, P. J. Gierasch, M. J. S. Belton, G. S. Orton, K. P. Klaasen, E. DeJong, H. H. Breneman, T. J. Jones, J. M. Kaufman, K. P. Magee, and D. A. Senske 1998. Galileo imaging of Jupiter's atmosphere: The Great Red Spot, equatorial region, and white ovals. *Icarus* **135**.

[45] Wallace, J.M., and Hobbs, P.V., 1977. Atmospheric Science: An Introductory Survey, 467 pp., Academic, San Diego, Calif.

[46] West, R. A., D. F. Strobel, and M. G. Tomasko 1986. Clouds, aerosols, and photochemistry in the jovian atmosphere. *Icarus* **65**.

[47] Yair, Y., Z. Levin, and S. Tzivion 1995. Lightning generation in a jovian thundercloud: Results from an axisymmetric numerical cloud model. *Icarus* **115**.

[48] Weidenschilling, S. J., and J. S. Lewis 1973. Atmospheric and cloud structures of the jovian planets. *Icarus* **20**.

[49] Figure 1. Little, B. et al. Galileo images of lightning on Jupiter. *Icarus* **142**, pp. 314 (1999).

[50] Figure 2. Gierasch, P.J. Ingersoll, A.P. Banfield, Ewald, S.P. Helfenstein, P. Simon-Miller, Vasavada, A. Breneman, H.H. Senske, D.A., and the Galileo Imaging Team. 2000. Observations of moist convection in Jupiter's atmosphere. *Nature* **403**, pp. 629.

[51] Figure 3. Gierasch, P.J. Ingersoll, A.P. Banfield, Ewald, S.P. Helfenstein, P. Simon-Miller, Vasavada, A. Breneman, H.H. Senske, D.A., and the Galileo Imaging Team. 2000. Observations of moist convection in Jupiter's atmosphere. *Nature* **403**, pp. 628.

[52] Figure 4. Marcus, P.S. 2004. Prediction of a global climate change on Jupiter. *Nature* **428**, pp. 828.

[53] Table 1. Little, B. et al. Galileo images of lightning on Jupiter. *Icarus* **142**, pp. 309 (1999).

[54] Table 2. Dyudina, U.A., A.P., Ingersoll, A. R. Vasavada, S. P. Ewald Galileo SSI Team. Monte Carlo Radiative Transfer Modeling of Lightning Observed in Galileo Images of Jupiter, *Icarus* **160**, pp. 345 (2002).